



1 **Nitrate formation from heterogeneous uptake of dinitrogen pentoxide during a severe**
2 **winter haze in southern China**

3 Hui Yun¹, Weihao Wang¹, Tao Wang^{1,*}, Men Xia¹, Chuan Yu^{1,2}, Zhe Wang¹, Steven C.N.
4 Poon¹, Dingli Yue³, Yan Zhou³

5 ¹Department of Civil and Environmental Engineering, The Hong Kong Polytechnic
6 University, Hong Kong, China

7 ²Environment Research Institute, Shandong University, Jinan, China

8 ³Guangdong Environmental Monitoring Center, State Environmental Protection Key
9 Laboratory of Regional Air Quality Monitoring, Guangzhou, China

10 *Correspondence to: Tao Wang (cetwang@polyu.edu.hk)

11 **Abstract:** Nitrate (NO_3^-) has become a major component of fine particulate matter ($\text{PM}_{2.5}$)
12 during hazy days in China. However, the role of the heterogeneous reactions of dinitrogen
13 pentoxide (N_2O_5) in nitrate formation is not well constrained. In January 2017, a severe haze
14 event occurred in the Pearl River Delta (PRD) of southern China during which high levels of
15 $\text{PM}_{2.5}$ ($\sim 400 \mu\text{g m}^{-3}$) and O_3 (~ 160 ppbv) were observed at a semi-rural site (Heshan) in the
16 western PRD. Nitrate concentrations were up to $108 \mu\text{g m}^{-3}$ (1 h time resolution), and the
17 contribution of nitrate to $\text{PM}_{2.5}$ reached nearly 40%. Concurrent increases in NO_3^- and ClNO_2
18 (with a maximum value of 8.3 ppbv in 1 min time resolution) were observed in the first
19 several hours after sunset, indicating an intense N_2O_5 heterogeneous uptake on aerosols. The
20 formation potential of NO_3^- via N_2O_5 heterogeneous reactions was estimated to be 39.7 to 77.3
21 $\mu\text{g m}^{-3}$ in the early hours (3 to 6 h) after sunset based on the measurement data, which could
22 completely explain the measured increase in the NO_3^- concentration during the same time
23 period. Daytime production of nitric acid from the gas-phase reaction of $\text{OH} + \text{NO}_2$ was
24 calculated with a chemical box model built using the Master Chemical Mechanism (MCM
25 v3.3.1) and constrained by the measurement data. The integrated nocturnal nitrate formed via
26 N_2O_5 chemistry was comparable to or even higher than the nitric acid formed during the
27 daytime. This study confirms that N_2O_5 heterogeneous chemistry was a significant source of
28 aerosol nitrate during hazy days in southern China.

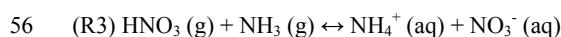
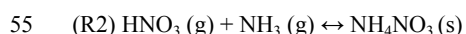
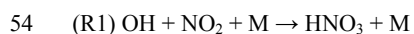
29 **Keywords:** N_2O_5 , ClNO_2 , nitrate, Pearl River Delta, southern China



30 1 Introduction

31 Severe haze in China has been a major concern of the regulatory and scientific communities
32 in recent years. Nitrate was identified as an important component of PM_{2.5} during hazy days
33 in both summer and winter (e.g., Huang et al., 2014; Li et al., 2018; Pathak et al., 2009;
34 Zhang et al., 2015). Moreover, the proportion of nitrate in PM_{2.5} has increased steadily in the
35 last decade due to the lagged control of NO_x emissions compared to SO₂ (Fu et al., 2014;
36 Geng et al., 2017; Qu et al., 2017; Reuter et al., 2014; Wang X et al., 2016). As a result, the
37 concentrations of nitrate in PM_{2.5}/PM_{1.0} were even higher than those of sulfate during some
38 haze events (Ge et al., 2017; Li et al., 2017; Liu et al., 2015; Yang et al., 2017; Yue et al.,
39 2015).

40 Nitrate is formed from NO_x in both the daytime and nighttime. During the day, nitric acid
41 (HNO₃) is produced through the gas-phase reaction between OH and NO₂ (R1), and this
42 pathway is insignificant at night due to very low OH concentrations (e.g., Seinfeld and Pandis,
43 2016). The nitric acid can react with ammonia (NH₃) to form ammonium nitrate (NH₄NO₃),
44 and an equilibrium can be reached for these three compounds between the gas phase and the
45 particle phase (R2-3). In the nighttime, heterogeneous uptake of N₂O₅, which is formed from
46 the reactions involving O₃, NO₂ and NO₃, becomes a source of nitrate and also produces
47 gaseous ClNO₂ when chloride-containing aerosol is present (R4-7) (Finlayson-Pitts et al.,
48 1989). This nitrate formation pathway is important only at night due to the fast photolysis of
49 NO₃ during the day. Compared to the relatively well-understood formation of aerosol nitrate
50 via the OH + NO₂ reaction, the contribution from N₂O₅ heterogeneous reactions has been
51 poorly quantified due to the limited knowledge of key factors controlling the heterogeneous
52 processes, such as the N₂O₅ uptake coefficient ($\gamma_{\text{N}_2\text{O}_5}$) and ClNO₂ yield (ϕ_{ClNO_2}) (Brown and
53 Stutz, 2012; Chang et al., 2011).





58 (R5) $\text{NO}_2 + \text{NO}_3 + \text{M} \leftrightarrow \text{N}_2\text{O}_5 + \text{M}$

59 (R6) $\text{NO}_3 + \text{VOCs} \rightarrow \text{products}$

60 (R7) $\text{N}_2\text{O}_5 + \text{H}_2\text{O}$ or $\text{Cl}^- (\text{aq}) \rightarrow (2-\phi) \text{NO}_3^- (\text{aq}) + \phi \text{ClNO}_2 (\text{g})$

61 Model studies initially treated $\gamma_{\text{N}_2\text{O}_5}$ as a constant (0.03 to 0.1) (Dentener and Crutzen,
62 1993;Makar et al., 1998;Munger et al., 1998;Schaap et al., 2004;Wen et al., 2015;Xue et al.,
63 2014), and later utilized several parameterization schemes of $\gamma_{\text{N}_2\text{O}_5}$ and ϕ_{ClNO_2} based on the
64 laboratory investigations of their dependence on aerosol compositions and aerosol water
65 content (Anttila et al., 2006;Bertram and Thornton, 2009;Davis et al., 2008;Evans and Jacob,
66 2005;Riemer et al., 2009;Riemer et al., 2003;Roberts et al., 2009). However, recent studies
67 found a significant discrepancy between the field-derived and parameterized $\gamma_{\text{N}_2\text{O}_5}$ and ϕ_{ClNO_2}
68 (McDuffie et al., 2018; Phillips et al., 2016; Tham et al., 2018; Wang X et al., 2017; Wang Z
69 et al., 2017; Zhou et al., 2018). These findings suggest that N_2O_5 uptake is more complicated
70 than previously thought and a better understanding of the uptake process is needed to improve
71 the prediction of nitrate and haze.

72 In addition to the modeling approach, field measurements of trace gases and aerosol
73 composition have been used to infer the contribution of N_2O_5 heterogeneous chemistry to
74 nitrate formation. Pathak et al. (2009) postulated the importance of N_2O_5 heterogeneous
75 reactions to the high aerosol nitrate observed in summertime in Beijing and Shanghai by
76 examining the variation of nitrate with the change in relative humidity (RH) and the
77 equilibrium between anions and cations in $\text{PM}_{2.5}$. Pathak et al. (2011) further investigated
78 nitrate formation using a coupled aqueous phase radical mechanism (CAPRAM) and a
79 gas-phase chemistry mechanism (RACM, without ClNO_2 chemistry). By constraining the
80 uptake coefficient of N_2O_5 in the range of 0.001 to 0.1, they reproduced the observed
81 enhancement of nitrate and suggested that N_2O_5 uptake in aerosols contributed to 50 to 100%
82 of the nighttime increase in nitrate. A similar method was used recently by Wen et al. (2018)
83 to simulate the summertime nitrate formation in the North China Plain (NCP), which
84 demonstrated the dominant contribution of N_2O_5 heterogeneous reactions to nighttime nitrate
85 formation. Based on the observed covariation of nitrate and RH, Wang et al. (2009)



86 speculated that N_2O_5 reactions dominated the nitrate formation on polluted days with high
87 NO_2 and O_3 in Shanghai. Neither N_2O_5 nor ClNO_2 was measured during these early
88 observation-based studies. A recent study (Wang H et al., 2017) inferred $\gamma_{\text{N}_2\text{O}_5}$ from the
89 measured N_2O_5 on four days in urban Beijing and estimated the lower limit of the formation
90 potential of aerosol nitrate assuming a unity ϕ_{ClNO_2} because ClNO_2 was not measured. Their
91 result showed a comparable contribution to nitrate formation from the N_2O_5 heterogeneous
92 chemistry as from the daytime pathway of the $\text{OH} + \text{NO}_2$ reaction.

93 In the present study, N_2O_5 , ClNO_2 , the related chemical and meteorological parameters were
94 measured at a semi-rural site in the Pearl River Delta of southern China from Jan 2 to Jan 15,
95 2017. A severe haze event was observed during the field study with $\text{PM}_{2.5}$ reaching $400 \mu\text{g m}^{-3}$
96 and O_3 up to 160 ppbv. ClNO_2 , which is only known to be produced from N_2O_5 heterogeneous
97 uptake, reached up to 8.3 ppbv, which is the highest ever reported value and revealed
98 extremely active N_2O_5 chemistry during the episode. The concurrent measurements of N_2O_5 ,
99 ClNO_2 and aerosol nitrate provide better constraints for elucidating nighttime $\text{NO}_3/\text{N}_2\text{O}_5$
100 chemistry and aerosol formation. An overview of the measurement data was first presented.
101 The nighttime processes that led to the formation of nitrate (e.g., production of NO_3 and N_2O_5 ,
102 N_2O_5 uptake coefficient, ClNO_2 yield) were analyzed. The nighttime formation potential of
103 nitrate was estimated based on these data and compared to the measured increase in nitrate.
104 The daytime production of nitric acid via the $\text{OH} + \text{NO}_2$ reaction was calculated based on a
105 box model using the Master Chemical Mechanism (MCM v3.3.1) and compared to the
106 nighttime formation potential of nitrate.

107 **2 Methods**

108 **2.1 Site description**

109 The field observation was conducted at the Guangdong Atmospheric Supersite, a semi-rural
110 site located at Hua Guo Shan (HGS, 22.728°N , 112.929°E) in the southwest of the city of
111 Heshan from Jan 2 to Jan 15, 2017. As shown in Fig. 1, HGS is a hill with a height of 60 m
112 above sea level. All measurement instruments were located on the 4th floor of a four-story
113 building on the top of the hill. The observation site was located in the western PRD where the



114 economic activity and population density are much less compared to central PRD. There are
115 five main roads near the HGS site, including three national roads (G325, G94 and G15), and
116 two provincial roads (S272 and S270). The hill is covered by subtropical trees and surrounded
117 by similar hills within close range, and a few residents live at the foot of the hill with some
118 farmland in the area.

119 2.2 Chemical ionization mass spectrometer

120 N_2O_5 and ClNO_2 were simultaneously observed using a quadrupole chemical ionization mass
121 spectrometer (THS Instruments, Atlanta) which converted N_2O_5 and ClNO_2 to ion clusters of
122 $\text{I}(\text{N}_2\text{O}_5)^+$ and $\text{I}(\text{ClNO}_2)^+$ (Tham et al., 2016; Wang T et al., 2016). Iodide ions (I^-) were
123 produced by exposing a mixture of $\text{CH}_3\text{I}/\text{N}_2$ (0.3%v/v) to an alpha radioactive source, 210-Po
124 (NRD, P-2031-2000). $\text{I}(\text{N}_2\text{O}_5)^+$ and $\text{I}(\text{ClNO}_2)^+$ were generated from the reaction between
125 $\text{I}(\text{H}_2\text{O})$ and $\text{N}_2\text{O}_5/\text{ClNO}_2$, and were detected at 235 and 208 m/z, respectively. The time
126 resolution for the measurement was approximately 10 s, and the derived data were later
127 averaged to a time resolution of 1 min for further analysis. Activated carbon packed in a filter
128 before the sampling inlet was used to determine the instrument background. The calibration of
129 N_2O_5 and ClNO_2 were carried out every afternoon at the site, and the standard gas of N_2O_5
130 was added into the ambient air every 3 h to check the changes of sensitivity. A more detailed
131 description of the operation method of the CIMS can refer to Wang T et al. (2016). The
132 detection limits of N_2O_5 and ClNO_2 were 7 pptv and 6 pptv (3σ , 1 min-averaged data),
133 respectively. The uncertainty and the precision of the measurement was $\pm 25\%$ and 3%,
134 respectively.

135 The inlet of the CIMS instrument was set approximately 1.5 m above the roof with 6 m long
136 PFA-Teflon tubing as the sampling line. The total sampling flow was set as 11 standard liters
137 per minute (SLPM). Four SLPM were diverted into the CIMS, O_3 and NO_x analyzer, and the
138 remaining part was evacuated directly from the system. The total residence time was less than
139 1 s in the sampling system. To reduce the influence of the tubing wall adhered with deposited
140 particles, we replaced the inlet tubing and fittings every day and washed them with an
141 ultrasonic bath.



142 2.3 Other measurements

143 Trace gases of CO, SO₂, O₃, NO_x, total reactive nitrogen (NO_y), nitrous acid (HONO), C₂ to
144 C₁₀ non-methane hydrocarbons (NMHCs) and oxygenated hydrocarbons (OVOCs) were
145 measured. CO was observed using a gas filter correlation analyzer (Thermo Model 48i). SO₂
146 was measured using a pulsed fluorescence analyzer (Thermo Model 43i). O₃ was determined
147 using a UV photometric analyzer (Thermo, Model 49i). NO and NO₂ were detected with a
148 special chemiluminescence instrument (Thermo, Model 42i). A photolytic converter only
149 sensitive to NO₂ was equipped in this instrument (Xu et al., 2013). NO_y was determined using
150 a general chemiluminescence analyzer (Thermo, Model 42i-Y) which was equipped with a
151 molybdenum oxide (MoO) catalytic converter. HONO was detected using a long path
152 absorption photometer (QUMA, Model LOPAP-03) (Xu et al., 2015). NMHCs were
153 determined using an online gas chromatograph (GC) coupled with a flame ionization detector
154 (FID) and a mass spectrometer (MS). NMHCs were only measured from Jan 2 to Jan 8, 2017
155 due to the maintenance of the GCMS after Jan 8. OVOCs (e.g., formaldehyde, acetaldehyde,
156 acetone, methyl ethyl ketone) were sampled with 2,4-dinitrophenylhydrazine cartridges every
157 3 h and were later analyzed with a high-performance liquid chromatography (HPLC) system
158 (Cui et al., 2016).

159 Concentrations of PM_{2.5} were detected with a multi-angle absorption photometer (MAAP,
160 Thermo Model 5012). The ionic compositions of PM_{2.5} were measured with an ion
161 chromatography (GAC-IC) system equipped with a gas and aerosol collector at a time
162 resolution of 30 min (Yue et al., 2015), and the data were also averaged every 1 h to meet the
163 time resolution of other components of PM_{2.5}. Organic carbon (OC) and elemental carbon (EC)
164 were measured with an online OC/EC analyzer (RT-4, SUNSET) with a time resolution of 1 h.
165 A scanning mobility particle sizer (SMPS Model 3936L75, TSI) was used to determine the
166 dry-state particle number size distribution, covering the size range from 16.5 to 1000 nm. The
167 ambient (wet) particle number size distributions were estimated based on a size-resolved
168 kappa-Köhler function considering the variation with the relative humidity (Hennig et al.,
169 2005; Liu et al., 2014). Aerosol surface density was then derived using the ambient particle
170 number size distribution (wet) and an assumption of spherical particles (Tham et al., 2016;



171 Wang Z et al., 2017).

172 Meteorological parameters were measured with a portable weather station (Model WXT520,
173 Vaisala, Finland), including temperature, relative humidity (RH), wind direction, wind speed,
174 and pressure. A pyranometer (CMP22, Kipp & Zonen B.V., Holland) was used to measure the
175 solar radiation and the data were then utilized to derive the photolysis frequency of NO₂ based
176 on the method of Trebs et al. (2009).

177 **2.4 Chemical box model**

178 To estimate the daytime formation of nitric acid via the reaction of OH + NO₂, an
179 observation-based chemical box model developed with the latest version of the Master
180 Chemical Mechanism v3.3.1 (Jenkin et al., 2003; Jenkin et al., 2015; Saunders et al., 2003)
181 and an updated chlorine (Cl) radical chemistry module (Xue et al., 2015) was utilized to
182 calculate the mixing ratio of OH radicals and the reaction rate of OH + NO₂. The integrated
183 production of nitric acid during the daytime was then calculated based on the simulation
184 results. The box model was constrained with the observation data every 10 min, including the
185 data of N₂O₅, ClNO₂, HONO, O₃, NO, NO₂, SO₂, CO, C₂ to C₁₀ NMHCs, OVOCs
186 (formaldehyde, acetaldehyde, acetone, and MEK), temperature, aerosol surface density and
187 $J(\text{NO}_2)$, which were first averaged or interpolated. Average concentrations of NMHC species
188 during the daytime (7:00 to 17:00) and nighttime (17:00 to 7:00 of the next day) are shown in
189 Table S1. A function considering the variation of the solar zenith angle (Saunders et al., 2003)
190 was used to calculate the photolysis frequencies of HONO, O₃ and other species in clear sky,
191 which were then corrected with the $J(\text{NO}_2)$ values in the real environment. The $J(\text{ClNO}_2)$ was
192 treated the same as in Tham et al. (2016). The lifetime of unconstrained species respect to the
193 physical loss was set as 8 h in a boundary layer of 1000 m depth (equivalent to $3.47 \times 10^{-5} \text{ s}^{-1}$)
194 in order to avoid their accumulation. The model was run from 0:00 of Jan 3 to 11:00 of Jan 8,
195 2017. To stabilize the intermediate species, the simulation for the first 24 h was repeated six
196 times.



197 3 Results and discussion

198 3.1 Overview of the observation

199 Figure 2 shows the time series of N_2O_5 , ClNO_2 , components of $\text{PM}_{2.5}$, related trace gases and
200 meteorological parameters from 18:40 of Jan 2 to 11:00 of Jan 15, 2017. The average
201 temperature and RH during the measurement period were $17 \pm 4^\circ\text{C}$ and $86 \pm 14\%$,
202 respectively. A severe pollution episode occurred on Jan 3 to 7 due to stagnant meteorological
203 conditions (Fig. 3 (a)), and the concentrations of most pollutants decreased to very low levels
204 on Jan 9 and Jan 12 to 15, which corresponded to the change in weather conditions. The most
205 polluted days were Jan 5 and 6 with the highest $\text{PM}_{2.5}$ of $400 \mu\text{g m}^{-3}$ and the highest O_3 of 160
206 ppbv. The $\text{PM}_{2.5}$ data from the PRD regional air quality monitoring network revealed that the
207 HGS site was within the most polluted area during this haze event (Fig. 3(b)). This pollution
208 event was characterized by concurrent high levels of $\text{PM}_{2.5}$ and O_3 and is in contrast to the
209 winter haze in north China, which experienced high $\text{PM}_{2.5}$ but low O_3 (e.g., Sun et al., 2016;
210 Wang H et al., 2018a). The mixing ratios of N_2O_5 and ClNO_2 were up to 3358 pptv and 8324
211 pptv (1 min time resolution), respectively, indicating active N_2O_5 heterogeneous chemistry.

212 Very high concentrations of aerosol nitrate (up to $108 \mu\text{g m}^{-3}$, 1 h time resolution) were also
213 observed during the multi-day episode. Nitrate contributed to 24% of the total $\text{PM}_{2.5}$ mass
214 concentration on average, which was comparable to that of organic matters ($\text{OM} = 1.7 \cdot \text{OC}$,
215 28%) and much higher than that of sulfate (16%) and ammonium (11%). The contribution of
216 nitrate to the $\text{PM}_{2.5}$ increased with an increase in nitrate concentration, and reached nearly 40%
217 at its highest nitrate level, indicating that nitrate was a dominant component of the $\text{PM}_{2.5}$ on
218 the most polluted days. The concentration of NO_3^- exhibited a concurrent increase with that of
219 ClNO_2 in the early nighttime on Jan 3 to 4, Jan 4 to 5, Jan 5 to 6 and Jan 9 to 10 (see Fig. 4),
220 suggesting that N_2O_5 heterogeneous reactions significantly contributed to the formation of
221 nitrate during the nighttime. The measured increases of the NO_3^- concentration during these
222 four nights were 35.3, 50.9, 43.3 and $32.7 \mu\text{g m}^{-3}$, respectively. A similar increase in ClNO_2
223 was observed on Jan 6 to 7, but the composition of the $\text{PM}_{2.5}$ was not available due to
224 instrument maintenance. The discussion in the remainder of this manuscript will focus on the
225 detailed analysis of these five nights to investigate the role of N_2O_5 heterogeneous chemistry



226 in nitrate formation.

227 **3.2 N₂O₅ heterogeneous chemistry on the selected nights**

228 **3.2.1 Production of NO₃ and N₂O₅**

229 The first step in the nighttime nitrate formation via N₂O₅ chemistry is the production of NO₃
230 and N₂O₅. To get insight into the key factors affecting the NO₃/N₂O₅ chemistry, the variation
231 of N₂O₅ and production rate of NO₃ were examined with some relevant gases and
232 meteorological parameters of the five nights. Fig. 5 shows the data of the night of Jan 4 to 5
233 as an example. Some common features were identified for all five nights. In general, low
234 wind speed (< 2.0 m s⁻¹) at night facilitated the accumulation of air pollutants, and high RH
235 was favorable for N₂O₅ heterogeneous uptake. In addition, high aerosol surface density
236 provided interfaces for N₂O₅ heterogeneous reactions.

237 In the first couple of hours after sunset (Fig 5, red rectangle), N₂O₅ exhibited a peak and
238 quickly dropped to hundreds of pptv, while nitrate and ClNO₂ concurrently increased, which
239 was indicative of the local production and loss of N₂O₅. NO was below the detection limit
240 during this period. The production rates of NO₃ ($P_{\text{NO}_3} = k_{\text{NO}_2+\text{O}_3}[\text{NO}_2][\text{O}_3]$) were the fastest
241 just after sunset and decreased gradually due to reduced O₃ levels. There was a period later in
242 the night (22:00 to 01:00) when fresh emissions of NO were observed, and the production of
243 NO₃ was suppressed due to the titration of O₃ by NO. In the later nighttime, NO was below
244 the detection limit (Fig. 5, blue rectangle). During this period, NO₃ and N₂O₅ were produced
245 at moderate rates, and the very low N₂O₅ concentrations (below the detection limit) suggested
246 a fast loss of N₂O₅ probably leading to the local production of ClNO₂ and nitrate, which was
247 not revealed in the observed variations of ClNO₂ and nitrate. The concentrations of ClNO₂
248 and nitrate during this period fluctuated due to the change in the air masses indicated by the
249 change in SO₂ concentrations and wind speeds.

250 **3.2.2 N₂O₅ uptake coefficient and ClNO₂ yield**

251 The N₂O₅ uptake coefficient and ClNO₂ yield, together with the reactivity of NO₃ with NO
252 and VOCs, determines the loss pathways of NO₃ and N₂O₅. To derive the uptake coefficient of
253 N₂O₅, a method suggested by McLaren et al. (2010) was applied by treating NO₃ and N₂O₅ as



254 a whole ($[\text{NO}_3] + [\text{N}_2\text{O}_5]$) without assuming the chemical system was in the steady state. This
 255 approach considers that the change of NO_3 and N_2O_5 concentrations is mainly due to
 256 $\text{NO}_3/\text{N}_2\text{O}_5$ chemistry, and thus it requires that the air mass have relatively stable chemical
 257 conditions and not be subject to fresh NO emissions. It also requires that ClNO_2 is produced
 258 from the N_2O_5 chemistry and has an increasing trend to derive the yield of ClNO_2 . This
 259 method is applicable for the early nighttime (red rectangle, section 3.2.1) for these five nights.

260 The variation rate of $[\text{NO}_3] + [\text{N}_2\text{O}_5]$ can be calculated by deducting the production rate of
 261 $[\text{NO}_3] + [\text{N}_2\text{O}_5]$ with its loss rate as Eq. (1).

$$262 \quad (1) \quad \frac{d([\text{N}_2\text{O}_5] + [\text{NO}_3])}{dt} = P_{\text{NO}_3} - L_{\text{N}_2\text{O}_5 + \text{NO}_3}$$

263 The loss of $[\text{NO}_3] + [\text{N}_2\text{O}_5]$ is through the NO_3 reaction with VOCs and N_2O_5 heterogeneous
 264 reactions, which can both be expressed as pseudo first order losses as Eq. (2):

$$265 \quad (2) \quad L_{\text{N}_2\text{O}_5 + \text{NO}_3} = L_{\text{NO}_3} + L_{\text{N}_2\text{O}_5} = k_{\text{NO}_3} [\text{NO}_3] + k_{\text{N}_2\text{O}_5} [\text{N}_2\text{O}_5]$$

266 where k_{NO_3} and $k_{\text{N}_2\text{O}_5}$ represent the total first order rate constants for NO_3 and N_2O_5 ,
 267 respectively. The loss rate of N_2O_5 can then be obtained from Eq. (3):

$$268 \quad (3) \quad L_{\text{N}_2\text{O}_5} = k_{\text{N}_2\text{O}_5} [\text{N}_2\text{O}_5] = k_{\text{NO}_2 + \text{O}_3} [\text{NO}_2][\text{O}_3] - \frac{d[\text{N}_2\text{O}_5]}{dt} - \frac{d[\text{NO}_3]}{dt} - k_{\text{NO}_3} [\text{NO}_3]$$

269 Because NO_3 was not measured, it was calculated by assuming an equilibrium of
 270 NO_2 - NO_3 - N_2O_5 as shown in Eq. (4). High levels of NO would break this equilibrium. Thus,
 271 the periods with detected NO were excluded. $d[\text{NO}_3]/dt$ and $d[\text{N}_2\text{O}_5]/dt$ were calculated as the
 272 rate of change of NO_3 and N_2O_5 in a time resolution of 10 min. k_{NO_3} was derived with the
 273 measured concentrations of NMHCs as Eq. (5) by interpolating the data of NMHCs to 10 min
 274 time resolution. The NO_3 reactivity with VOCs (k_{NO_3}) in the early nighttime ranged from
 275 0.632 to $1.54 \times 10^{-3} \text{ s}^{-1}$ (Table 1), which was higher than those derived at Mt. TMS in winter
 276 2013 (0.17 to $1.1 \times 10^{-3} \text{ s}^{-1}$) (Brown et al., 2016), but lower than those in the North China Plain
 277 during the summertime (2 - $57 \times 10^{-3} \text{ s}^{-1}$) (Tham et al., 2016; Wang H et al., 2017, 2018b; Wang
 278 Z et al., 2017). NMHCs were not measured on Jan 9 to 10, 2017. Therefore, we used the
 279 average k_{NO_3} in the early nighttime on Jan 3 to 4 as a replacement because these two periods



280 had similar pollution levels for most pollutants. For the later nighttime (Fig. 5, blue rectangle),
 281 low levels of N_2O_5 and moderate levels of P_{NO_3} also made Eq. (3) inapplicable even though
 282 NO was not detected.

$$283 \quad (4) \quad [NO_3] = \frac{[N_2O_5]}{[NO_2] \times K_{eq}}$$

$$284 \quad (5) \quad k_{NO_3} = \sum k_i [VOC_i]$$

285 Finally, the uptake coefficient of N_2O_5 was derived using Eq. (6) for every 10 min and
 286 averaged for the whole selected periods. In Eq. (6), $C_{N_2O_5}$ is the mean molecular speed of
 287 N_2O_5 , and S_a is the aerosol surface density. The yield of $ClNO_2$ was derived from Eq. (7) by
 288 dividing the integrated production of $ClNO_2$ ($[ClNO_2]_{max}$) to the integrated loss of N_2O_5 since
 289 sunset.

$$290 \quad (6) \quad k_{N_2O_5} = \frac{L_{N_2O_5}}{[N_2O_5]} = \frac{1}{4} C_{N_2O_5} S_a \gamma_{N_2O_5}$$

$$291 \quad (7) \quad \phi = \frac{[ClNO_2]_{max}}{\int L_{N_2O_5} dt}$$

292 The relative importance of NO_3 reactions with VOCs and N_2O_5 heterogeneous reactions can
 293 be examined by comparing the values of the loss coefficient of NO_3 reactions ($\frac{k_{NO_3}}{[NO_2] \times K_{eq}}$) and
 294 N_2O_5 heterogeneous reactions ($k_{N_2O_5}$) (Tham et al., 2016). Based on the calculations, the
 295 values of $\frac{k_{NO_3}}{[NO_2] \times K_{eq}}$ were 1.82×10^{-5} to $6.07 \times 10^{-5} \text{ s}^{-1}$ (see Table 1), while that of $k_{N_2O_5}$ were
 296 3.78×10^{-3} to $20.4 \times 10^{-3} \text{ s}^{-1}$, which was two orders of magnitude higher than that of $\frac{k_{NO_3}}{[NO_2] \times K_{eq}}$,
 297 suggesting that N_2O_5 heterogeneous reactions were the dominant loss pathway of NO_3 and
 298 N_2O_5 .

299 The average $\gamma_{N_2O_5}$ and ϕ_{ClNO_2} derived for the early night of the five cases are listed in Table 1.
 300 The data show that the uptake coefficient ranged from 0.009 to 0.101, which was comparable
 301 to the previous values derived at Mt. Tai Mo Shan (TMS) in Hong Kong (0.004 to 0.022)
 302 (Brown et al., 2016) and in the North China Plain (0.006 to 0.102) (Tham et al., 2018; Tham
 303 et al., 2016; Wang H et al., 2017, 2018b; Wang X et al., 2017; Wang Z et al., 2017; Zhou et al.,
 304 2018). The yield in this study varied from 0.20 to 0.36, which was similar to most studies in



305 China (Tham et al., 2018; Tham et al., 2016; Wang Z et al., 2017; Yun et al., 2018; Zhou et al.,
306 2018).

307 3.3 Nitrate formation potential ($p(\text{NO}_3^-)$) through N_2O_5 chemistry

308 3.3.1 Nighttime $p(\text{NO}_3^-)$

309 The formation potential of NO_3^- through N_2O_5 chemistry is the total amount of NO_3^-
310 accumulated from N_2O_5 heterogeneous loss. It can be calculated by deducting the integrated
311 loss of N_2O_5 with the integrated production of ClNO_2 as Eq. (8).

$$312 \text{ (Eq.8) } p(\text{NO}_3^-) = (2-\phi) \int L_{\text{N}_2\text{O}_5} dt = 2 \int L_{\text{N}_2\text{O}_5} dt - [\text{ClNO}_2]_{\text{max}}$$

313 In the early nighttime, the average loss rate of N_2O_5 ($L_{\text{N}_2\text{O}_5}$) ranged from 1.9 to 3.9 ppbv h^{-1}
314 (Table 1), which was close to the average P_{NO_3} due to the dominance of the N_2O_5
315 heterogeneous reactions in NO_3 and N_2O_5 loss. Based on the derived N_2O_5 loss rate and the
316 maximum ClNO_2 concentration, the formation potential of NO_3^- was derived and ranged from
317 39.7 to 77.3 $\mu\text{g m}^{-3}$ as shown in Fig. 6. The measured increase of the NO_3^- concentration in the
318 early nighttime can be completely explained by the integrated production of NO_3^- via the
319 N_2O_5 heterogeneous reactions during the same period.

320 In the later nighttime, the method described in section 3.2.2 was not valid for calculating the
321 N_2O_5 heterogeneous loss rate as mentioned above. We attempted to estimate the formation
322 potential of nitrate by assuming that the N_2O_5 heterogeneous reactions continued to dominate
323 the loss of $\text{NO}_3 + \text{N}_2\text{O}_5$ in the later nighttime. The k_{NO_3} in the later nighttime were comparable
324 to those in the early nighttime, and the high RH close to 100% in the later nighttime was
325 favorable for the N_2O_5 heterogeneous reactions. We assumed that all NO_3 was quickly
326 consumed by the N_2O_5 heterogeneous reactions, which means that the loss rate of N_2O_5
327 approximated to the production rate of NO_3 ($L_{\text{N}_2\text{O}_5} \approx P_{\text{NO}_3}$). As listed in Table 2, the N_2O_5 loss
328 rates ranged from 0.82 to 1.26 ppbv h^{-1} , which were significantly lower than those derived in
329 the early nighttime. The derived N_2O_5 loss rate here and the yield of ClNO_2 in the early
330 nighttime were used to estimate the formation potential of NO_3^- in the later nighttime. As
331 shown in Fig.6, the nitrate produced during these later periods ranged from 7.3 to 37.7 $\mu\text{g m}^{-3}$,



332 which was significantly lower than those in the early nighttime, indicating that the nighttime
333 nitrate from N_2O_5 chemistry was mainly produced in the early nighttime.

334 3.3.2 Comparison with daytime production of HNO_3

335 During the daytime, the formation of NO_3^- is mainly from the gas-particle partitioning of the
336 gas phase HNO_3 formed through the $\text{OH} + \text{NO}_2$ reaction. Hence, the daytime formation
337 potential of HNO_3 ($p(\text{HNO}_3)$) can be treated as the upper limit for the locally-produced
338 daytime aerosol nitrate. To calculate the daytime $p(\text{HNO}_3)$, a box model based on MCM
339 v3.3.1 was used to derive the mixing ratio of OH and the rates of $\text{OH} + \text{NO}_2$ as described in
340 section 2.4. This model was previously used in our study at Wangdu in North China (Tham et
341 al., 2016). The calculated mixing ratios of OH at Wangdu with this model compared well with
342 those observed by the laser-induced fluorescence (LIF) technique (Tan et al., 2017). In the
343 present study, the average daytime OH (7:00 to 17:00) mixing ratios were 1.71 to 3.82×10^6
344 cm^{-3} during Jan 3 to 7 as listed in Table 3 with the maximum values reaching 3.24 to 6.71×10^6
345 cm^{-3} . The detailed results for OH can be found in Fig. S1.

346 The average production rates of HNO_3 through the $\text{OH} + \text{NO}_2$ reaction were 1.40 to 5.21 ppbv
347 h^{-1} from Jan 3 to Jan 7, and the integrated formation potential of HNO_3 during the daytime
348 was 35.7 to $131.8 \mu\text{g m}^{-3}$, which was comparable to the nighttime $p(\text{NO}_3^-)$ ranging from 77.4
349 to $102.9 \mu\text{g m}^{-3}$ (Fig. 7). Nighttime production of nitrate via the heterogeneous uptake of N_2O_5
350 accounted for 43.8 to 57.7% of the total nitrate ($\text{NO}_3^- + \text{HNO}_3$) produced in a 24 h period at
351 the site. These results underscored the important role of N_2O_5 heterogeneous chemistry in
352 nitrate formation in this severe winter haze in southern China.

353 4 Concluding remarks

354 With the use of concurrent measurements of nitrate, ClNO_2 and related pollutants, this study
355 demonstrates the important contribution of N_2O_5 heterogeneous uptake in nitrate formation.
356 Current chemical transport models have difficulties in simulating this nitrate production
357 pathway. Therefore, more research efforts are needed to improve the representations of $\gamma_{\text{N}_2\text{O}_5}$
358 and ϕ_{ClNO_2} for better prediction of nitrate in the models. The observation-based approach
359 presented here can be applied to investigate nitrate formation in other areas of China.



360 **5 Data availability**

361 The data used in this study are available from the corresponding author upon request
362 (cetwang@polyu.edu.hk & dingliyue@163.com).

363 **Acknowledgment**

364 The authors thank Dr. Li Qinyi and Dr. Fu Xiao for helpful discussions, and Miss Yaru Wang
365 and Yiheng Liang for their help in analyzing the OVOC and aerosol composition. This study
366 was supported by the Hong Kong Research Grants Council (HK-RGC; C5022-14G and
367 PolyU 153026/14P) and National Natural Science Foundation (NNSF) of China (91544213).
368 Z. Wang acknowledges the support of the NNSF of China (41505103) and HK-RGC
369 (25221215).

370 **References**

- 371 Anttila, T., Kiendler-Scharr, A., Tillmann, R., and Mentel, T. F.: On the reactive uptake of gaseous
372 compounds by organic-coated aqueous aerosols: Theoretical analysis and application to the
373 heterogeneous hydrolysis of N_2O_5 , *The Journal of Physical Chemistry A*, 110, 10435-10443, 2006.
- 374 Bertram, T., and Thornton, J.: Toward a general parameterization of N_2O_5 reactivity on aqueous
375 particles: the competing effects of particle liquid water, nitrate and chloride, *Atmos Chem Phys*, 9,
376 8351-8363, 2009.
- 377 Brown, S. S., and Stutz, J.: Nighttime radical observations and chemistry, *Chem Soc Rev*, 41,
378 6405-6447, 2012.
- 379 Brown, S. S., Dubé, W. P., Tham, Y. J., Zha, Q., Xue, L., Poon, S., Wang, Z., Blake, D. R., Tsui, W.,
380 and Parrish, D. D.: Nighttime Chemistry at a High Altitude Site Above Hong Kong, *J. Geophys.*
381 *Res. Atmos.*, 121, 2457–2475, doi: 10.1002/2015JD024566, 2016.
- 382 Chang, W. L., Bhave, P. V., Brown, S. S., Riemer, N., Stutz, J., and Dabdub, D.: Heterogeneous
383 Atmospheric Chemistry, Ambient Measurements, and Model Calculations of N_2O_5 : A Review,
384 *Aerosol Sci Tech*, 45, 665-695, doi:10.1080/02786826.2010.551672, 2011.
- 385 Cui, L., Zhang, Z., Huang, Y., Lee, S. C., Blake, D. R., Ho, K. F., Wang, B., Gao, Y., Wang, X. M., and
386 Louie, P. K. K.: Measuring OVOCs and VOCs by PTR-MS in an urban roadside
387 microenvironment of Hong Kong: relative humidity and temperature dependence, and field
388 intercomparisons, *Atmos Meas Tech*, 9, 5763-5779, 2016.
- 389 Davis, J. M., Bhave, P. V., and Foley, K. M.: Parameterization of N_2O_5 reaction probabilities on the
390 surface of particles containing ammonium, sulfate, and nitrate, *Atmos Chem Phys*, 8, 5295-5311,
391 2008.
- 392 Dentener, F. J., and Crutzen, P. J.: Reaction of N_2O_5 on tropospheric aerosols: Impact on the global
393 distributions of NO_x , O_3 , and OH, *J. Geophys. Res. Atmos.*, 98, 7149-7163, 1993.
- 394 Evans, M. J., and Jacob, D. J.: Impact of new laboratory studies of N_2O_5 hydrolysis on global model
395 budgets of tropospheric nitrogen oxides, ozone, and OH, *Geophys. Res. Lett.*, 32, L09813, doi:



- 396 10.1029/2005GL022469, 2005.
- 397 Finlayson-Pitts, B. J., Ezell, M. J., and Pitts, J. N.: Formation of chemically active chlorine compounds
398 by reactions of atmospheric NaCl particles with gaseous N₂O₅ and ClONO₂, *Nature*, 337, 241-244,
399 1989.
- 400 Fu, X., Wang, X., Guo, H., Cheung, K., Ding, X., Zhao, X., He, Q., Gao, B., Zhang, Z., and Liu, T.:
401 Trends of ambient fine particles and major chemical components in the Pearl River Delta region:
402 observation at a regional background site in fall and winter, *Sci Total Environ*, 497, 274-281,
403 2014.
- 404 Ge, X., He, Y., Sun, Y., Xu, J., Wang, J., Shen, Y., and Chen, M.: Characteristics and formation
405 mechanisms of fine particulate nitrate in typical urban areas in China, *Atmosphere*, 8, 62, 2017.
- 406 Geng, G., Zhang, Q., Tong, D., Li, M., Zheng, Y., Wang, S., and He, K.: Chemical composition of
407 ambient PM_{2.5} over China and relationship to precursor emissions during 2005-2012, *Atmos.*
408 *Chem. Phys*, 17, 9187-9203, 2017.
- 409 Hennig, T., Massling, A., Brechtel, F., and Wiedensohler, A.: A tandem DMA for highly
410 temperature-stabilized hygroscopic particle growth measurements between 90% and 98% relative
411 humidity, *J Aerosol Sci*, 36, 1210-1223, 2005.
- 412 Huang, R. J., Zhang, Y. L., Bozzetti, C., Ho, K. F., Cao, J. J., Han, Y. M., Daellenbach, K. R., Slowik, J.
413 G., Platt, S. M., Canonaco, F., Zotter, P., Wolf, R., Pieber, S. M., Bruns, E. A., Crippa, M., Ciarelli,
414 G., Piazzalunga, A., Schwikowski, M., Abbaszade, G., Schnelle-Kreis, J., Zimmermann, R., An, Z.
415 S., Szidat, S., Baltensperger, U., El Haddad, I., and Prevot, A. S. H.: High secondary aerosol
416 contribution to particulate pollution during haze events in China, *Nature*, 514, 218-222, Doi:
417 10.1038/Nature13774, 2014.
- 418 Jenkin, M. E., Saunders, S. M., Wagner, V., and Pilling, M. J.: Protocol for the development of the
419 Master Chemical Mechanism, MCM v3 (Part B): tropospheric degradation of aromatic volatile
420 organic compounds, *Atmos Chem Phys*, 3, 181-193, 2003.
- 421 Jenkin, M. E., Young, J. C., and Rickard, A. R.: The MCM v3.3.1 degradation scheme for isoprene,
422 *Atmos Chem Phys*, 15, 11433-11459, 2015.
- 423 Li, H., Zhang, Q., Zheng, B., Chen, C., Wu, N., Guo, H., Zhang, Y., Zheng, Y., Li, X., and He, K.:
424 Nitrate-driven urban haze pollution during summertime over the North China Plain, *Atmos Chem*
425 *Phys*, 18, 5293-5306, 2018.
- 426 Li, W., Liu, X., Zhang, Y., Sun, K., Wu, Y., Xue, R., Zeng, L., Qu, Y., and An, J.: Characteristics and
427 formation mechanism of regional haze episodes in the Pearl River Delta of China, *Journal of*
428 *Environmental Sciences*, 63, 236-249, 2017.
- 429 Liu, H., Zhao, C., Nekat, B., Ma, N., Wiedensohler, A., Van Pinxteren, D., Spindler, G., Müller, K., and
430 Herrmann, H.: Aerosol hygroscopicity derived from size-segregated chemical composition and its
431 parameterization in the North China Plain, *Atmos Chem Phys*, 14, 2525-2539, 2014.
- 432 Liu, X., Sun, K., Qu, Y., Hu, M., Sun, Y., Zhang, F., and Zhang, Y.: Secondary formation of sulfate and
433 nitrate during a haze episode in megacity Beijing, China, *Aerosol Air Qual. Res*, 15, 2246-2257,
434 2015.
- 435 Makar, P., Wiebe, H., Staebler, R., Li, S., and Anlauf, K.: Measurement and modeling of particle nitrate
436 formation, *J. Geophys. Res. Atmos.*, 103, 13095-13110, 1998.
- 437 McDuffie, E. E., Fibiger, D. L., Dubé, W. P., Lopez-Hilfiker, F., Lee, B. H., Thornton, J. A., Shah, V.,
438 Jaeglé, L., Guo, H., and Weber, R. J.: Heterogeneous N₂O₅ uptake during winter: Aircraft
439 measurements during the 2015 WINTER campaign and critical evaluation of current



- 440 parameterizations, *J. Geophys. Res. Atmos.*, 123, 4345-4372, doi: 10.1002/2018JD028336, 2018.
- 441 McLaren, R., Wojtal, P., Majonis, D., McCourt, J., Halla, J. D., and Brook, J.: NO₃ radical
442 measurements in a polluted marine environment: links to ozone formation, *Atmos. Chem. Phys.*,
443 10, 4187-4206, 2010.
- 444 Munger, J. W., Fan, S. M., Bakwin, P. S., Goulden, M. L., Goldstein, A., Colman, A. S., and Wofsy, S.
445 C.: Regional budgets for nitrogen oxides from continental sources: Variations of rates for
446 oxidation and deposition with season and distance from source regions, *J. Geophys. Res. Atmos.*,
447 103, 8355-8368, 1998.
- 448 Pathak, R. K., Wu, W. S., and Wang, T.: Summertime PM_{2.5} ionic species in four major cities of China:
449 Nitrate formation in an ammonia-deficient atmosphere, *Atmos Chem Phys*, 9, 1711-1722, 2009.
- 450 Pathak, R. K., Wang, T., and Wu, W. S.: Nighttime enhancement of PM_{2.5} nitrate in ammonia-poor
451 atmospheric conditions in Beijing and Shanghai: Plausible contributions of heterogeneous
452 hydrolysis of N₂O₅ and HNO₃ partitioning, *Atmos Environ*, 45, 1183-1191,
453 doi:10.1016/j.atmosenv.2010.09.003, 2011.
- 454 Phillips, G. J., Thieser, J., Tang, M., Sobanski, N., Schuster, G., Fachinger, J., Drewnick, F., Borrmann,
455 S., Bingemer, H., and Lelieveld, J.: Estimating N₂O₅ uptake coefficients using ambient
456 measurements of NO₃, N₂O₅, ClNO₂ and particle-phase nitrate, *Atmos Chem Phys*, 16,
457 13231-13249, 2016.
- 458 Qu, Z., Henze, D. K., Capps, S. L., Wang, Y., Xu, X., Wang, J., and Keller, M.: Monthly top-down NO_x
459 emissions for China (2005–2012): A hybrid inversion method and trend analysis, *J. Geophys. Res.*
460 *Atmos.*, 122, 4600-4625, 2017.
- 461 Reuter, M., Buchwitz, M., Hilboll, A., Richter, A., Schneising, O., Hilker, M., Heymann, J.,
462 Bovensmann, H., and Burrows, J.: Decreasing emissions of NO_x relative to CO₂ in East Asia
463 inferred from satellite observations, *Nat Geosci*, 7, 792, 2014.
- 464 Riemer, N., Vogel, H., Vogel, B., Schell, B., Ackermann, I., Kessler, C., and Hass, H.: Impact of the
465 heterogeneous hydrolysis of N₂O₅ on chemistry and nitrate aerosol formation in the lower
466 troposphere under photosmog conditions, *J. Geophys. Res.*, 108, 4144, doi:
467 10.1029/2002JD002436, D4, 2003.
- 468 Riemer, N., Vogel, H., Vogel, B., Anttila, T., Kiendler - Scharr, A., and Mentel, T.: Relative importance
469 of organic coatings for the heterogeneous hydrolysis of N₂O₅ during summer in Europe, *J.*
470 *Geophys. Res.*, 114, D17307, doi: 10.1029/2008JD011369, 2009.
- 471 Roberts, J. M., Osthoff, H. D., Brown, S. S., Ravishankara, A., Coffman, D., Quinn, P., and Bates, T.:
472 Laboratory studies of products of N₂O₅ uptake on Cl-containing substrates, *Geophys. Res. Lett.*,
473 36, L20808, doi: 10.1029/2009GL040448, 2009.
- 474 Saunders, S. M., Jenkin, M. E., Derwent, R. G., and Pilling, M. J.: Protocol for the development of the
475 Master Chemical Mechanism, MCM v3 (Part A): tropospheric degradation of non-aromatic
476 volatile organic compounds, *Atmos Chem Phys*, 3, 161-180, 2003.
- 477 Schaap, M., Loon, M. v., Ten Brink, H., Dentener, F., and Builtjes, P.: Secondary inorganic aerosol
478 simulations for Europe with special attention to nitrate, *Atmos Chem Phys*, 4, 857-874, 2004.
- 479 Seinfeld, J. H., and Pandis, S. N.: Atmospheric chemistry and physics: from air pollution to climate
480 change, John Wiley & Sons, 2016.
- 481 Sun, Y., Chen, C., Zhang, Y., Xu, W., Zhou, L., Cheng, X., Zheng, H., Ji, D., Li, J., and Tang, X.: Rapid
482 formation and evolution of an extreme haze episode in Northern China during winter 2015,
483 *Scientific reports*, 6, 27151, 2016.



- 484 Tan, Z., Fuchs, H., Lu, K., Hofzumahaus, A., Bohn, B., Broch, S., Dong, H., Gomm, S., Häseler, R., He,
485 L., Holland, F., Li, X., Liu, Y., Lu, S., Rohrer, F., Shao, M., Wang, B., Wang, M., Wu, Y., Zeng, L.,
486 Zhang, Y., Wahner, A., and Zhang, Y.: Radical chemistry at a rural site (Wangdu) in the North
487 China Plain: observation and model calculations of OH, HO₂ and RO₂ radicals, *Atmos. Chem.*
488 *Phys.*, 17, 663-690, [10.5194/acp-17-663-2017](https://doi.org/10.5194/acp-17-663-2017), 2017.
- 489 Tham, Y. J., Wang, Z., Li, Q., Yun, H., Wang, W., Wang, X., Xue, L., Lu, K., Ma, N., Bohn, B., Li, X.,
490 Kecorius, S., Größ, J., Shao, M., Wiedensohler, A., Zhang, Y., and Wang, T.: Significant
491 concentrations of nitryl chloride sustained in the morning: investigations of the causes and impacts
492 on ozone production in a polluted region of northern China, *Atmos. Chem. Phys.*, 16,
493 14959-14977, [doi:10.5194/acp-16-14959-2016](https://doi.org/10.5194/acp-16-14959-2016), 2016.
- 494 Tham, Y. J., Wang, Z., Li, Q., Wang, W., Wang, X., Lu, K., Ma, N., Yan, C., Kecorius, S., Wiedensohler,
495 A., Zhang, Y., and Wang, T.: Heterogeneous N₂O₅ uptake coefficient and production yield of
496 ClNO₂ in polluted northern China: Roles of aerosol water content and chemical composition,
497 *Atmos. Chem. Phys. Discuss.*, [doi:10.5194/acp-2018-313](https://doi.org/10.5194/acp-2018-313), 2018.
- 498 Trebs, I., Bohn, B., Ammann, C., Rummel, U., Blumthaler, M., Königstedt, R., Meixner, F., Fan, S.,
499 and Andreae, M.: Relationship between the NO₂ photolysis frequency and the solar global
500 irradiance, *Atmos Meas Tech*, 2, 725-739, 2009.
- 501 Wang, H., Lu, K., Chen, X., Zhu, Q., Chen, Q., Guo, S., Jiang, M., Li, X., Shang, D., Tan, Z., Wu, Y.,
502 Wu, Z., Zou, Q., Zheng, Y., Zeng, L., Zhu, T., Hu, M., and Zhang, Y.: High N₂O₅ Concentrations
503 Observed in Urban Beijing: Implications of a Large Nitrate Formation Pathway, *Environmental*
504 *Science & Technology Letters*, [doi:10.1021/acs.estlett.7b00341](https://doi.org/10.1021/acs.estlett.7b00341), 2017.
- 505 Wang, H., Lu, K., Chen, X., Zhu, Q., Wu, Z., Wu, Y., and Sun, K.: Large particulate nitrate formation
506 from N₂O₅ uptake in a chemically reactive layer aloft during winter time in Beijing, *Atmos. Chem.*
507 *Phys. Discuss.*, [doi:10.5194/acp-2017-1217](https://doi.org/10.5194/acp-2017-1217), 2018a.
- 508 Wang, H., Lu, K., Guo, S., Wu, Z., Shang, D., Tan, Z., Wang, Y., Le Breton, M., Zhu, W., Lou, S., Tang,
509 M., Wu, Y., Zheng, J., Zeng, L., Hallquist, M., Hu, M., and Zhang, Y.: Efficient N₂O₅ Uptake and
510 NO₃ Oxidation in the Outflow of Urban Beijing, *Atmos. Chem. Phys. Discuss.*,
511 [doi:10.5194/acp-2018-88](https://doi.org/10.5194/acp-2018-88), 2018b.
- 512 Wang, T., Tham, Y. J., Xue, L., Li, Q., Zha, Q., Wang, Z., Poon, S. C., Dubé, W. P., Blake, D. R., and
513 Louie, P. K.: Observations of nitryl chloride and modeling its source and effect on ozone in the
514 planetary boundary layer of southern China, *J. Geophys. Res. Atmos.*, 121, 2476–2489, [doi:](https://doi.org/10.1002/2015JD024556)
515 [10.1002/2015JD024556](https://doi.org/10.1002/2015JD024556), 2016.
- 516 Wang, X., Zhang, Y., Chen, H., Yang, X., Chen, J., and Geng, F.: Particulate nitrate formation in a
517 highly polluted urban area: a case study by single-particle mass spectrometry in Shanghai,
518 *Environ Sci Technol*, 43, 3061-3066, 2009.
- 519 Wang, X., Chen, W., Chen, D., Wu, Z., and Fan, Q.: Long-term trends of fine particulate matter and
520 chemical composition in the Pearl River Delta Economic Zone (PRDEZ), China, *Frontiers of*
521 *Environmental Science & Engineering*, 10, 53-62, 2016.
- 522 Wang, X., Wang, H., Xue, L., Wang, T., Wang, L., Gu, R., Wang, W., Tham, Y. J., Wang, Z., Yang, L.,
523 Chen, J., and Wang, W.: Observations of N₂O₅ and ClNO₂ at a polluted urban surface site in North
524 China: High N₂O₅ uptake coefficients and low ClNO₂ product yields, *Atmos Environ*, 156,
525 125-134, 2017.
- 526 Wang, Z., Wang, W., Tham, Y. J., Li, Q., Wang, H., Wen, L., Wang, X., and Wang, T.: Fast
527 heterogeneous N₂O₅ uptake and ClNO₂ production in power plant and industrial plumes observed



- 528 in the nocturnal residual layer over the North China Plain, *Atmos. Chem. Phys.*, 17, 12361-12378,
529 doi:10.5194/acp-17-12361-2017, 2017.
- 530 Wen, L., Chen, J., Yang, L., Wang, X., Xu, C., Sui, X., Yao, L., Zhu, Y., Zhang, J., and Zhu, T.:
531 Enhanced formation of fine particulate nitrate at a rural site on the North China Plain in summer:
532 The important roles of ammonia and ozone, *Atmos Environ*, 101, 294-302, 2015.
- 533 Wen, L., Xue, L., Wang, X., Xu, C., Chen, T., Yang, L., Wang, T., and Wang, W.: Summertime fine
534 particulate nitrate pollution in the North China Plain: Increasing trends, formation mechanisms,
535 and implications for control policy, *Atmos. Chem. Phys. Discuss.*, 2018, 1-27,
536 doi:10.5194/acp-2018-89, 2018.
- 537 Xu, Z., Wang, T., Xue, L. K., Louie, P. K. K., Luk, C. W. Y., Gao, J., Wang, S. L., Chai, F. H., and
538 Wang, W. X.: Evaluating the uncertainties of thermal catalytic conversion in measuring
539 atmospheric nitrogen dioxide at four differently polluted sites in China, *Atmos Environ*, 76,
540 221-226, 2013.
- 541 Xu, Z., Wang, T., Wu, J., Xue, L., Chan, J., Zha, Q., Zhou, S., Louie, P. K. K., and Luk, C. W. Y.:
542 Nitrous acid (HONO) in a polluted subtropical atmosphere: Seasonal variability, direct vehicle
543 emissions and heterogeneous production at ground surface, *Atmos Environ*, 106, 100-109, 2015.
- 544 Xue, J., Yuan, Z., Lau, A. K., and Yu, J. Z.: Insights into factors affecting nitrate in PM_{2.5} in a polluted
545 high NO_x environment through hourly observations and size distribution measurements, *J.*
546 *Geophys. Res. Atmos.*, 119, 4888-4902, 2014.
- 547 Xue, L. K., Saunders, S. M., Wang, T., Gao, R., Wang, X. F., Zhang, Q. Z., and Wang, W. X.:
548 Development of a chlorine chemistry module for the Master Chemical Mechanism, *Geoscientific*
549 *Model Development*, 8, 3151-3162, 2015.
- 550 Yang, T., Sun, Y., Zhang, W., Wang, Z., Liu, X., Fu, P., and Wang, X.: Evolutionary processes and
551 sources of high-nitrate haze episodes over Beijing, *Spring, Journal of Environmental Sciences*, 54,
552 142-151, 2017.
- 553 Yue, D., Zhong, L., Zhang, T., Shen, J., Zhou, Y., Zeng, L., Dong, H., and Ye, S.: Pollution properties
554 of water-soluble secondary inorganic ions in atmospheric PM_{2.5} in the Pearl River Delta region,
555 *Aerosol Air Qual. Res.*, 15, 1737-1747, 2015.
- 556 Yun, H., Wang, T., Wang, W., Tham, Y. J., Li, Q., Wang, Z., and Poon, S. C. N.: Nighttime NO_x loss
557 and ClNO₂ formation in the residual layer of a polluted region: Insights from field measurements
558 and an iterative box model, *Sci Total Environ*, 622-623, 727-734, 2018.
- 559 Zhang, R., Wang, G., Guo, S., Zamora, M. L., Ying, Q., Lin, Y., Wang, W., Hu, M., and Wang, Y.:
560 Formation of Urban Fine Particulate Matter, *Chemical Reviews*, 115, 3803-3855, doi:
561 10.1021/acs.chemrev.5b00067, 2015.
- 562 Zhou, W., Zhao, J., Ouyang, B., Mehra, A., Xu, W., Wang, Y., Bannan, T. J., Worrall, S. D., Priestley,
563 M., Bacak, A., Chen, Q., Xie, C., Wang, Q., Wang, J., Du, W., Zhang, Y., Ge, X., Ye, P., Lee, J. D.,
564 Fu, P., Wang, Z., Worsnop, D., Jones, R., Percival, C. J., Coe, H., and Sun, Y.: Production of N₂O₃
565 and ClNO₂ in summer in urban Beijing, China, *Atmos. Chem. Phys. Discuss.*,
566 doi:10.5194/acp-2018-349, 2018.
- 567
- 568
- 569



570 Table 1. Average values of N_2O_5 concentrations, N_2O_5 uptake coefficients, ClNO_2 yields and
 571 other related parameters and maximum values of ClNO_2 concentrations in the early nighttime
 572 for five selected nights.

Date	N_2O_5 pptv	Max- ClNO_2 pptv	NO_2 ppbv	O_3 ppbv	RH %	Sa $\mu\text{m}^2\text{cm}^{-3}$	P_{NO_3} ppbv h^{-1}	k_{NO_3} 10^{-3}s^{-1}	$\text{L}_{\text{N}_2\text{O}_5}$ ppbv h^{-1}	$k_{\text{NO}_3}/(\text{K}_{\text{eq}}[\text{NO}_2])$ 10^{-5}s^{-1}	$k_{\text{N}_2\text{O}_5}$ 10^{-3}s^{-1}	$\gamma_{\text{N}_2\text{O}_5}$	ϕ_{ClNO_2}
Jan.3 17:40-20:50	102	3145	22	68	68	3644	4.0	0.632	3.9	3.26	20.4	0.101	0.36
Jan 4 17:00-22:00	700	4608	24	61	82	6452	3.3	1.54	3.2	6.07	4.16	0.009	0.32
Jan 5 17:00-22:00	338	4828	18	73	81	8399	3.4	0.790	3.3	4.06	9.00	0.015	0.29
Jan 6 17:00-22:40	326	2908	13	82	77	5092	2.8	0.677	2.6	4.95	3.78	0.013	0.20
Jan 9 19:00-00:20	121	2553	19	41	85	5173	1.9	0.632	1.9	1.82	4.28	0.015	0.28

573

574 Table 2. Average values of N_2O_5 loss rate and related parameters for selected periods in the
 575 later nighttime.

Date	NO_2 ppbv	O_3 ppbv	P_{NO_3} ppbv h^{-1}	k_{NO_3} 10^{-3}s^{-1}	$\text{L}_{\text{N}_2\text{O}_5}$ ppbv h^{-1}
Jan 3-4 21:00-05:00	20.8	20.7	1.00	0.684	1.00
Jan 5 01:30-06:50	22.4	19.5	0.96	1.45	0.96
Jan 5-6 23:40-01:10	21.1	25.5	1.26	1.13	1.26
Jan 6-7 23:00-06:00	22.1	14.4	0.82	0.709	0.82
Jan 10 01:50-03:30	24.8	15.6	0.90	/	0.90

576

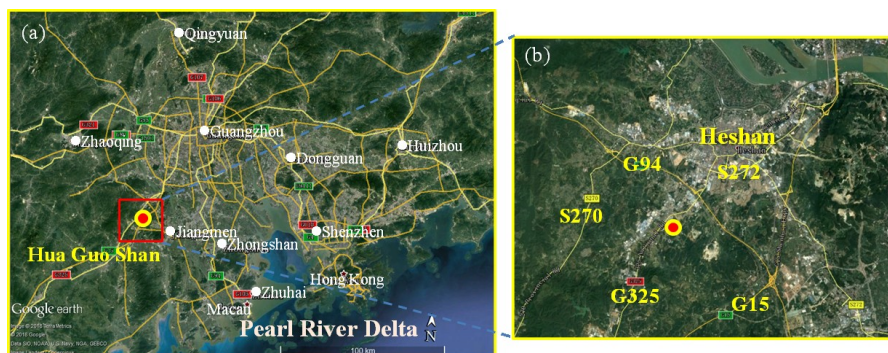
577 Table 3. Average OH mixing ratio and rate of $\text{OH} + \text{NO}_2$ during the daytime (7:00 to 17:00 LT)
 578 from Jan 3 to Jan 7, 2017.

Date	OH (cm^{-3})	NO_2 (ppbv)	$\text{OH} + \text{NO}_2$ (ppbv h^{-1})
Jan 3	2.18×10^6	36.2	3.49
Jan 4	2.47×10^6	23.6	2.60
Jan 5	2.62×10^6	30.8	3.09
Jan 6	3.82×10^6	31.5	5.21
Jan 7	1.71×10^6	18.4	1.40

579

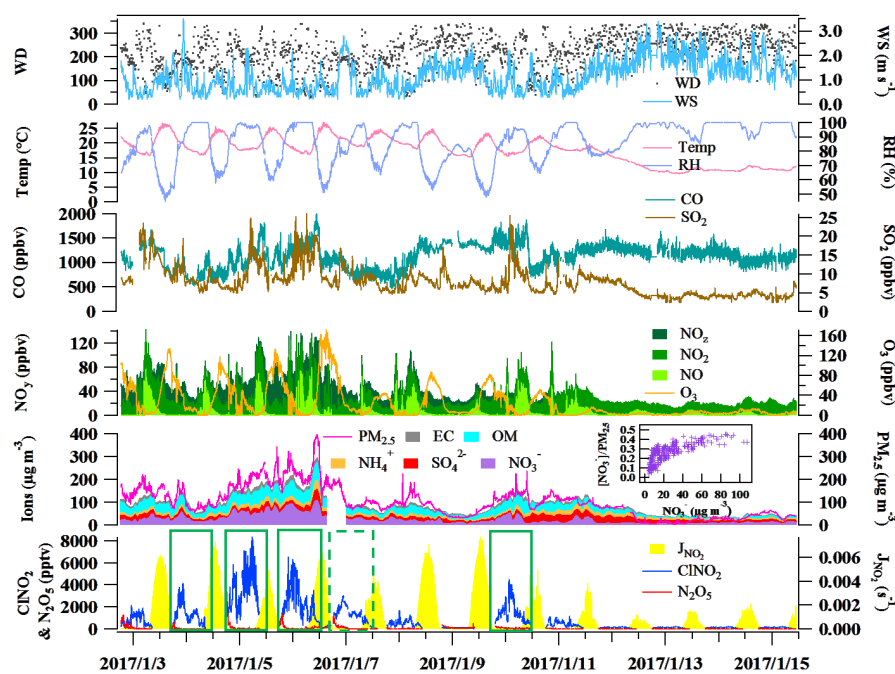
580

581



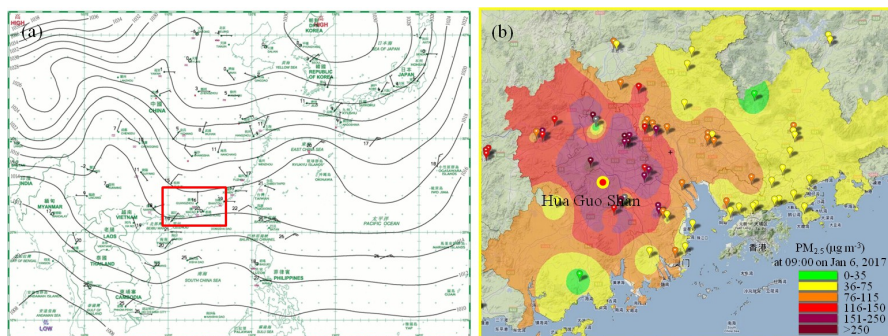
582

583 Figure 1. (a) Google map images of the Pearl River Delta in the Guangdong Province and
 584 measurement site (Hua Guo Shan). (b) The topography and major roads (shown by number)
 585 adjacent to the measurement site.

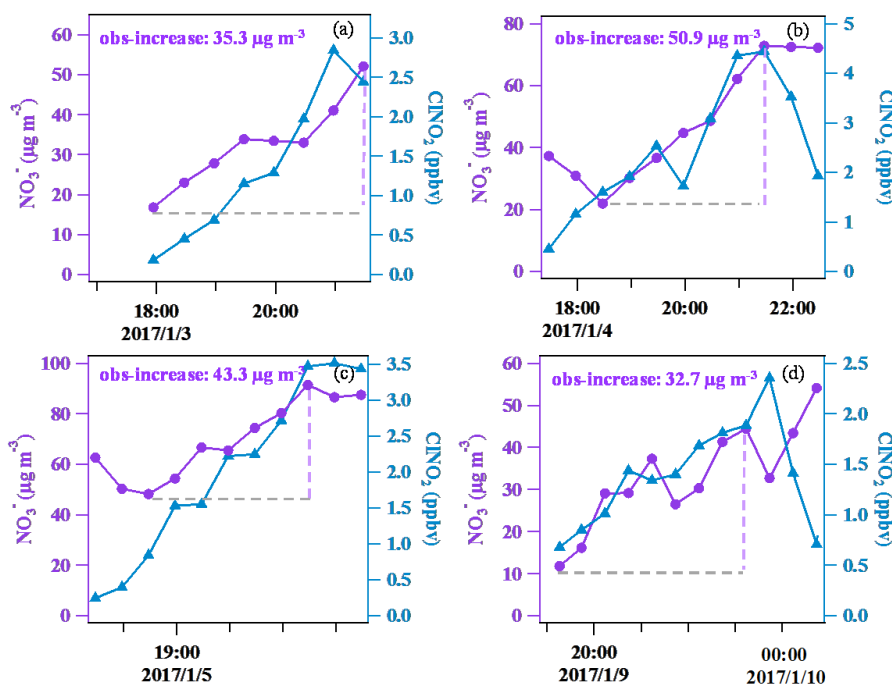


586

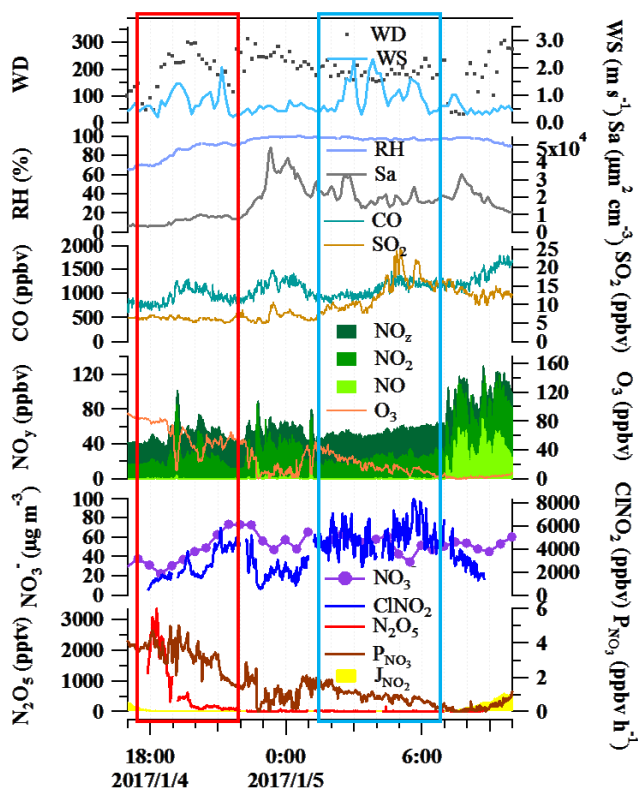
587 Figure 2. Time series of N_2O_5 , ClNO_2 , components of $\text{PM}_{2.5}$, related trace gases and
 588 meteorological parameters from 18:40 of Jan 2 to 11:00 of Jan 15, 2017. The inserted figure
 589 shows the variation of the ratio of nitrate to $\text{PM}_{2.5}$ with increasing nitrate concentration. The
 590 green rectangles in the figure indicate the five days used for detailed analysis.



591
 592 Figure 3. (a) Surface weather chart at 08:00 LT on Jan 6, 2017 downloaded from the website
 593 of the Hong Kong Observatory indicating stagnant conditions. (b) The distribution of $PM_{2.5}$
 594 concentrations in the PRD region at 09:00 LT on Jan 6, 2017. This figure was captured from
 595 the website. <http://113.108.142.147:20031/GDPublish/publish.aspx>.

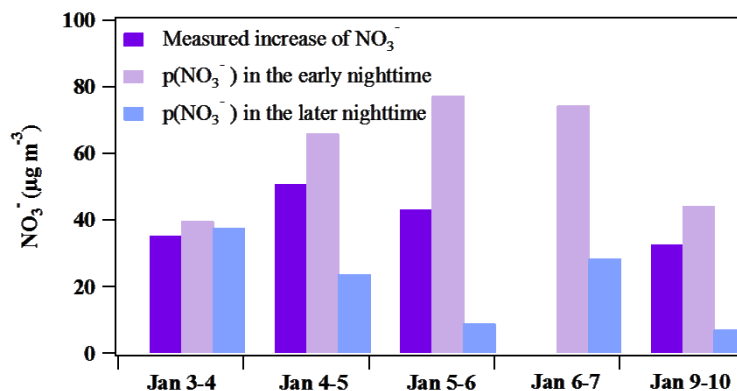


596
 597 Figure 4. The covariance of aerosol nitrate and $ClNO_2$ in the early nighttime (in 30 min time
 598 resolution) for four nights.



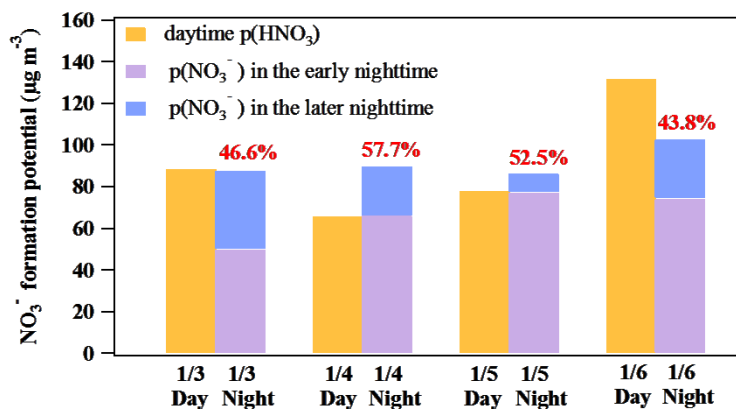
599

600 Figure 5. Variation of N_2O_5 , ClONO_2 , NO_3^- , trace gases and meteorological conditions during
 601 the nighttime of Jan 4 to 5, 2017 as an example for the five selected nights.



602

603 Figure 6. Comparison between the measured NO_3^- increase and the NO_3^- formation potential
 604 in the early nighttime (periods in Table 1) and in the later nighttime (periods in Table 2).



605

606 Figure 7. Comparison between the daytime (7:00 to 17:00 LT, assuming all gas phase HNO₃

607 partitioned into particle phase) and nighttime (17:00 to 7:00 LT of the next day) NO₃⁻

608 formation potential.

609